Dynamics and Ordering in Mixed Model Membranes of Dimyristoylphosphatidylcholine and Dimyristoylphosphatidylserine: A 250-GHz Electron Spin Resonance Study Using Cholestane

Jeff P. Barnes and Jack H. Freed
Baker Laboratory of Chemistry, Cornell University, Ithaca, New York 14853-1301 USA

ABSTRACT We report here on a 250-GHz electron spin resonance (ESR) study of macroscopically aligned model membranes composed of mixtures of dimyristoylphosphatidylcholine (DMPC) and dimyristoylphosphatidylserine (DMPS), utilizing the nixtroxide-labeled cholesterol analog cholestane (CSL). Two clearly resolved spectral components, distinct in both their ordering and dynamics, are resolved. The major component in membranes composed mostly of DMPC shows typical characteristics, with the long axis of CSL parallel to the bilayer normal with slow ($10^6 \leq R \leq 10^7\ s^{-1}$) rotational diffusion rates, as expected for cholesterol. The second component grows in as the mole fraction of DMPS increases. A detailed analysis shows that CSL senses a local, strongly biaxial environment. Our results imply that the inefficient packing between cholesterol and DMPS occurs probably because of the strong interactions between the PS headgroups, which provide the local biaxiality. Such a packing of the headgroups has been predicted by molecular dynamics simulations but had not been observed experimentally. The analysis of these spectral components was greatly aided by the excellent orientational resolution provided by the 250-GHz spectra. This enabled the key qualitative features of this interpretation to be "read" off the spectra before the detailed analysis.

INTRODUCTION

In this paper we present a far-infrared (FIR) electron spin resonance (ESR) study at 250 GHz and 9 Telsa of oriented model membranes containing mixtures of DMPC and DMPS. The primary virtue of FIR-ESR over ESR at conventional microwave frequencies is the excellent orientational resolution that it provides to studies utilizing nitroxide spin labels (Budil et al., 1989; Earle et al., 1997). However, it was very difficult in the past to study biologically relevant samples because of the relatively small FIR wavelengths (1.22 mm in this work) and the need to keep the lossy aqueous sample in a very small region where the FIR electric field is negligible. Such technical problems have now been solved (Barnes and Freed, 1997), and studies of membranes containing spin labels as well as spin-labeled proteins are now possible. These new techniques also enable us to study macroscopically aligned membrane samples, for which the orientational resolution is much greater.

The high resolution of both ordering and dynamics available with this new technique allows for a more detailed examination of the interactions between the various components of phospholipid membranes at the molecular level than was previously possible. For this first study, we have chosen a relatively simple system of DMPC/DMPS mixed model membranes, with the cholesterol-like spin label CSL that has frequently been utilized for studying the ordering and dynamics of cholesterol within the bilayers (Marriott et al., 1975; Kar et al., 1985; Shin and Freed, 1989; Shin et al., 1993; Ge et al., 1994a,b). This enables us to conveniently explore the new capabilities provided by FIR-ESR while studying a biologically interesting system, as discussed below.

Understanding the physical-chemical interactions between the diverse components of a biological membrane is important, because evidence has accumulated for their role in the regulation of cellular processes (Adam and Delbrück, 1968; Simons, 1997; McLaughlin and Aderem, 1995). Regulation can be achieved through specific, strong lipid/protein interactions or through multiple, weak lipid/lipid and lipid/protein interactions. It is these weaker interactions that are of interest here.

The cytosolic leaflet of the plasma membranes of many mammalian cells are actively enriched in the negatively charged lipid phosphatidylserine (PS) (Zachowski, 1993). Electrostatic attraction between these PS lipids and positively charged proteins is one way to bind proteins to membranes. This binding will also influence the membrane; for example, upon association of protein kinase C (PKC) to vesicles, PS has been observed by fluorescence digital imaging microscopy to aggregrate into domains beneath PKC (Yang and Glaser, 1995). In some cases, these induced domains are stable enough to be removed and purified along with the protein that induced them (Balvers et al., 1993). Within these domains, rotational motions of the hydrocarbon chains can be reduced (Kleinschmidt and Marsh, 1997) and the phospholipid headgroup orientations can be altered (Roux et al., 1989). Clearly, lipid/lipid interactions within a protein-induced domain can influence the energetics of protein/membrane association. For example, if a lipid were present that tended to prevent aggregration of PS in the membrane (e.g., there is a negative free energy of mixing between this lipid and PS), then the free energy of the PKC

Received for publication 6 March 1998 and in final form 28 July 1998.
Address reprint requests to Dr. Jack H. Freed, Department of Chemistry, Cornell University, B52 Baker Lab, Ithaca, NY 14853-1301. Tel.: 607-255-3647; Fax: 607-255-0595; E-mail: jhf@msc.cornell.edu.

0006-3495/98/11/2532/15 $2.00

binding would be lowered, because the negative charge in the membrane just below the PKC would not be as great as in the absence of the hypothetical lipid.

A second protein/lipid interaction is the classic hydrophobic effect (Tanford, 1991). Many proteins are posttranslationally modified by the addition of myristate to their amino-terminal glycine. This fatty acid chain inserts itself into the bilayer upon membrane association (Vergères et al., 1995). Lipids in the membrane may play a role in the regulation of this effect as well (Simons, 1997). In fact, the interaction between the hydrophobic moieties of proteins and bilayer lipids has been found to be quite complex, involving distinct binding sites for different lipids (Dreger et al., 1997), or altering the ordering and dynamics of the hydrocarbon chains in the bilayer for some distance around the protein (Mou et al., 1996; Patyal et al., 1997). This last effect may lead to a nonspecific, lipid-modulated attraction between membrane-associated proteins (Sintes and Baumgärtner, 1997), although for peripheral, electrostatically bound proteins its effect appears to be small (Heimburg and Marsh, 1995).

The interest in the present study is how cholesterol could influence either of these mechanisms. Cholesterol is present in both leaflets of the plasma membrane of many mammalian cells, although the degree of transmembrane asymmetry is a matter of some debate (Zachowski, 1993; Brasaemle et al., 1988). It is known to have many effects on membrane properties, including inhibiting the lateral segregation of certain mixtures of phospholipids (Silvius, 1992), inducing a separate phase with properties intermediate between those of the L_α and the gel phase (Recktenwald and McConnell, 1981; Ipsen et al., 1987) and increasing the ordering of the hydrocarbon chains in the L_α phase while decreasing it in the gel phase (Shin et al., 1993; Kar et al., 1985; Shin and Freed, 1989; Ipsen et al., 1987). The influence of cholesterol on the headgroup ordering/dynamics is less well characterized. NMR studies have been interpreted as showing the near independence of the headgroup dynamics from the hydrocarbon chain dynamics (Yeagle, 1991), although one might expect the incorporation of cholesterol into the bilayer to have some effect, because cholesterol has been shown to influence headgroup packing and hydration (Wachtel et al., 1991). Any of these effects could conceivably alter protein/lipid interactions.

ESR is a very useful spectroscopic technique to examine these effects; for example, the nonideal mixing of cholesterol in bilayers of hydrated DMPC was measured by detecting the change in the ordering of CSL and of chain-labeled lipids as a function of added cholesterol (Shin et al., 1993), and in unsaturated PC/PS bilayers it was found that a greater disordering at the ends of the hydrocarbon chains occurred for 1:1 PC:PS mixtures than for either pure PC or pure PS, suggesting the importance of headgroup interactions to hydrocarbon chain packing, even in the L_α phase (Ge et al., 1994b; Feigenson, 1989). Although many studies of the influence of a positively charged protein on PS-containing bilayers have been performed, the influence of cholesterol upon these induced domains has not yet been well characterized. One model system of these domains consists of bilayers of DMPC, progressively enriched in DMPS, for which a small amount of cholestane is added to act as a probe of the ordering and dynamics of cholesterol. We have the dual goals of 1) demonstrating that high-frequency (FIR) ESR represents a very sensitive spectroscopic method of determining molecular ordering and dynamics in membranes, and thereby reporting on lipid/lipid interactions, and 2) reporting on an unusual dynamical ordering of CSL in DMPS membranes not observed previously and suggesting its implications for cholesterol/lipid interactions in PS-rich domains.

EXPERIMENTAL

Sample preparation

The phospholipids 1,2-dimyristoyl-*sn*-glycero-3-phosphatidylcholine (DMPC) and 1,2-dimyristoyl-*sn*-glycero-3-phosphatidylserine (DMPS, Na^+ salt) were both obtained from Avanti Polar Lipids and were used without further purification. Stock solutions of DMPC in $CHCl_3$ and of DMPS in a 1:1 (v/v) mixture of $CHCl_3$ to CH_3OH were used to prepare solutions for ultracentrifugation. The spin probe 3β-doxyl-5α-cholestane (CSL) was obtained from Sigma Chemical Company and was used without further purification. A stock solution of CSL in $CHCl_3$ was used throughout this study.

Macroscopically aligned model membranes were made by the method of isopotential spin-dry ultracentrifugation (ISDU) (Clark et al., 1980; Ge et al., 1994a). Aliquots of the stock solutions were mixed to produce solutions with known molar fractions of DMPC to DMPS. Finally, an aliquot of the stock solution of CSL was added to create a 3:97 CSL-to-phospholipid ratio. We found no concentration-dependent line broadening from electron spin-spin interactions in our samples for CSL concentrations of 3 mol% or less, implying that the solutions are sufficiently dilute to prevent significant interactions between CSL molecules. Concentrations above 3 mol% CSL do, however, lead to an observable broadening of the 9-GHz ESR spectra, but not the 250 GHz spectra, because of spin-spin interactions. The rest of the sample preparation is as described previously (Ge et al., 1994a).

After ultracentrifugation, and again after recording ESR spectra, the samples were checked by polarizing microscopy to determine their degree of alignment. We searched for both a uniform texture (Asher and Pershan, 1979) and the presence of birefringence as determined by an interference pattern (Powers and Clark, 1975). Because the samples were 20–50 μm thick, the interference patterns had a low contrast, but could still be observed and always indicated the presence of a uniaxial phase (Powers and Clark, 1975). After warming the samples to above 45°C in the $\Psi = 0°$ resonator, polygonal defects were sometimes observed (cf. below). Warming to above 35°C in the $\Psi = 90°$ resonator for which the samples are in a vertical position often created oily streaks, indicating that some flow had occurred. Thus we mainly studied the gel phase.

Samples with defects observed immediately after ISDU alignment were rejected from further study. Occasionally, small crystals ~10 μm in diameter were observed after ISDU alignment, presumably because of excess salt from the DMPS. ESR spectra were still collected for these samples because the crystals appeared to create no misalignment, they never amounted to more than a few percent of the total surface area of the aligned membranes, and they did not dissolve upon warming of the samples to 30°C. The ESR data were always recorded starting at 10°C and as the samples were warmed to higher temperatures, so that the gel-phase ESR spectra would be trustworthy, even if the samples spontaneously disordered at the higher temperatures.

The borosilicate glass coverslips used for past 9-GHz ESR studies of ISDU aligned model membranes were found to be too lossy for 250-GHz

ESR. Instead, 12-mm-diameter quartz coverslips (ESCO Products) were used. The more fragile quartz always cracked when it was pressed against the curved bottom plate of the ISDU apparatus during ultracentrifugation. It was necessary to fabricate a flat-bottom plate to produce the ISDU samples. The ISDU sample radius is 0.377 cm, and the isopotential surface of the spinning bucket has a radius of curvature of 13.97 cm, so using a flat-bottom plate results in the bilayers being tilted upward at the sample's edge by 1.6°, which is not considered significant for these studies.

After samples were removed from the ultracentrifuge and checked under the microscope, they were weighed and then placed in a 100% relative humidity chamber at 20°C. For DMPC-rich membranes, the sample weight reached equilibrium after less than 24 h, at which point there were ~40 H_2O/phospholipid. Samples rich in DMPS could not be humidified for more than 48 h, because they would continue to collect water until they formed unilamellar vesicles (Hauser, 1984). Instead, these samples were allowed to absorb water for 24–48 h. The greatest hydration observed for any sample was 64 H_2O/phospholipid, for which the bilayer structure still exists (Hauser, 1984). The average degree of hydration for the samples used is shown in Table 1. After hydration, a quartz coverslip with an etched-in circular depression to accommodate the membrane was placed over the top of the sample. The sides of the quartz plates were sealed with a thin ring of (Dow Corning) silicone high-vacuum grease, which never touched the membrane sample. The top quartz plate also did not touch the membrane surface, to prevent the formation of defects. The samples were then kept in the dark at 10°C until they could be examined by ESR, but were allowed to sit at 20°C for at least 2 h to avoid the possibility of being in the pseudocrystalline-laminar (or L_c) phase (Marsh, 1988).

Spectrometer

The quasioptical techniques that have been utilized to construct and successfully operate an ESR spectrometer at 250 GHz at Cornell have been reviewed elsewhere (Budil et al., 1989; Earle et al., 1996). The design and implementation of the sample holder used for hydrated samples for high-frequency ESR have also been discussed (Barnes and Freed, 1997).

ESR spectra were recorded with the membrane normal (the direction $\hat{n}$) parallel and then perpendicular to the static magnetic field $\vec{B}_0$ (the case of $\Psi = 0°$ and 90°, respectively). The first orientation was obtained in a Fabry-Perot transmission-mode resonator (Barnes and Freed, 1997). For the second sample configuration, a "shunt" Fabry-Perot resonator was used in which the cylindrical axis of symmetry of the beam mode in the resonator was perpendicular to the axis of the optiguide. The details of this resonator are discussed elsewhere (Barnes and Freed, 1998). The same sample was used for both resonators as well as for 9-GHz ESR, as long as it was judged to have remained aligned by polarizing microscopy after the ESR data were collected. In general, however, thermal cycling destroyed the alignment of these samples.

A small degree of contamination of the DMPS with Mn^{2+} was detected with 250-GHz ESR. The splitting of the Mn^{2+} lines is 92 G, with a peak-to-peak linewidth of 9 G, which can be compared with a splitting of 92 G and a linewidth of 8 G found for a room-temperature aqueous solution of 0.6 mM $MnSO_4$, suggesting that most of the Mn^{2+} exists in, or exchanges rapidly with, the aqueous space between the bilayer surfaces. The concentration is $<2 \times 10^{-4}$ Mn^{2+} per phospholipid, which is low enough that the change in the average headgroup orientation of the phospholipids due to the Mn^{2+} would be nearly undetectable by ^2H NMR (see figure 6 of Roux and Bloom, 1990). In fact, the sharp signals from Mn^{2+} were found to be very useful as field markers, and they can be cleanly subtracted when necessary.

TABLE 1 The waters of hydration per phospholipid and the populations of the two distinct motional/ordering modes of CSL as a function of membrane composition

Composition % DMPC	Hydration H_2O:PC+PS	% DMPC-like component	Linewidth (Gauss)	% DMPS-like component
80	45	94	4	6
63	60	57	6	43
40	65	39	8	61
20	50	28	7	72
0	40	7	4	92

The width of the g_{yy} peak of the DMPC-like component was measured to see if exchange between the two components could be detected.

RESULTS

Fig. 1 shows a series of 250-GHz ESR spectra of ISDU membranes, fully hydrated, for $\Psi = 0°$, obtained at 10°C for which the membranes are in the gel phase. 250-GHz ESR spectra with $\Psi = 90°$ under otherwise identical conditions are shown in Fig. 2. In Fig. 3, we show the 250-GHz ESR spectra for a DMPC-rich (*top*) and a DMPS-rich (*bottom*) membrane at $\Psi = 0°$ out to 60°C. In passing through the gel to liquid-crystal phase temperature ($T_m = 23°C$ for DMPC and 45°C for DMPS), a sharpening of the linewidth of CSL in DMPC can be observed for the $\Psi = 0°$ spectrum. However, the main features of the lineshapes for either membrane composition do not change, suggesting that much of what we learn from the gel phase is applicable to the liquid crystalline phase, a matter we hope to confirm in future studies.

In Fig. 4 are shown the 9-GHz ESR spectra at 10°C of CSL in an 80:20 mol% DMPC:DMPS sample (*top*) and in a 20:80 mol% DMPC:DMPS sample (*bottom*), recorded for both $\Psi = 0°$ and 90°. The lineshape from the DMPS-rich sample is broad and would be difficult to interpret by itself. The reason for this will be discussed after the analysis of the 250-GHz ESR lineshapes.

ANALYSIS AND INTERPRETATION

We divide this section into two parts. In the first part we discuss how to interpret the high-frequency ESR spectra

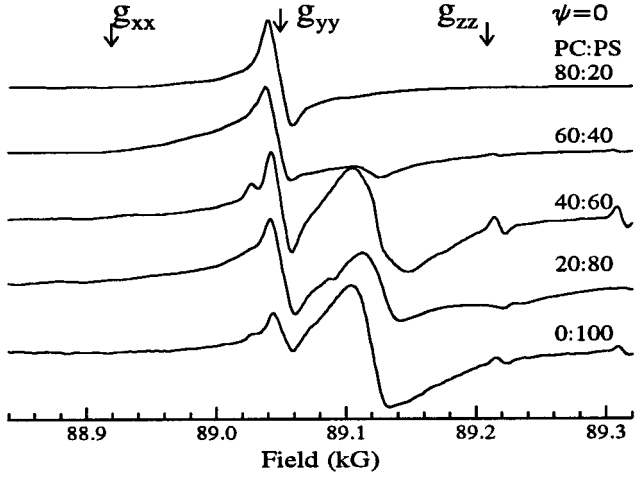

FIGURE 1 250-GHz ESR spectra of the $\Psi = 0°$ case for various compositions of the ISDU aligned and fully hydrated model membranes. All spectra were recorded at 10°C in the gel phase.

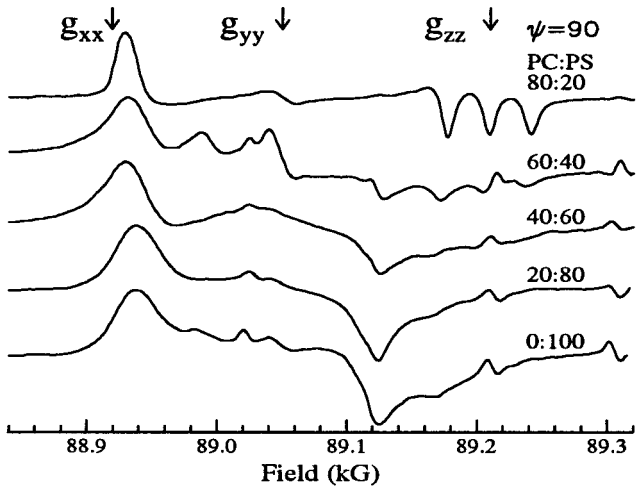

FIGURE 2 250 GHz ESR spectra of the $\Psi = 90°$ case for various compositions of the ISDU aligned and fully hydrated model membranes. All spectra were recorded at 10°C in the gel phase.

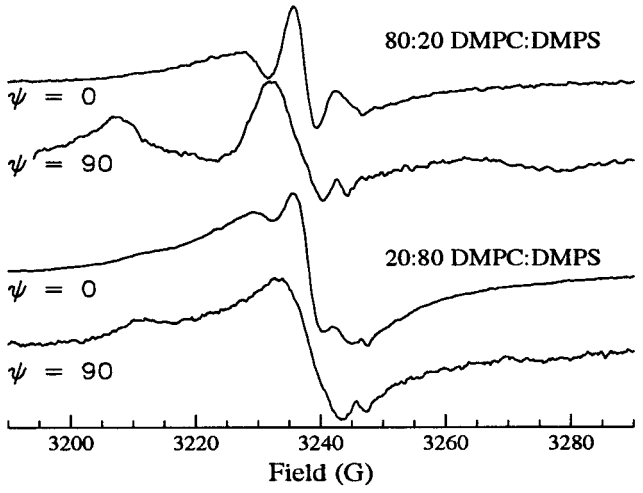

FIGURE 4 9.1-GHz ESR spectra at both $\Psi = 0°$ and 90° for ISDU-aligned model membranes prepared in the same way as the 250-GHz ESR samples and held in the same sample holder. The two compositions show some differences, but interpreting these without the 250-GHz data would be difficult (see text for details).

from a qualitative point of view. That is, we consider the features of the 250-GHz ESR lineshapes that provide qualitative insights on the ordering and rotational diffusional rates of CSL. The physical model suggested by these insights is then used as a starting point for a quantitative, least-squares fit to the ESR lineshape (Budil et al., 1996). In the second part, we give the details of several motional models that implemented, in varying degrees, the physical model developed in the first part, and discuss how successful they are in fitting the experimental lineshapes. In addition, we discuss how to improve the existing motional models contained in our simulation package, to better account for the features of the physical model. In the following discussion section we review some of what is known about the structure and dynamics of phospholipid membranes, with the goal of determining which interactions are primarily responsible for the unusual ordering of CSL in the DMPS-containing model membranes.

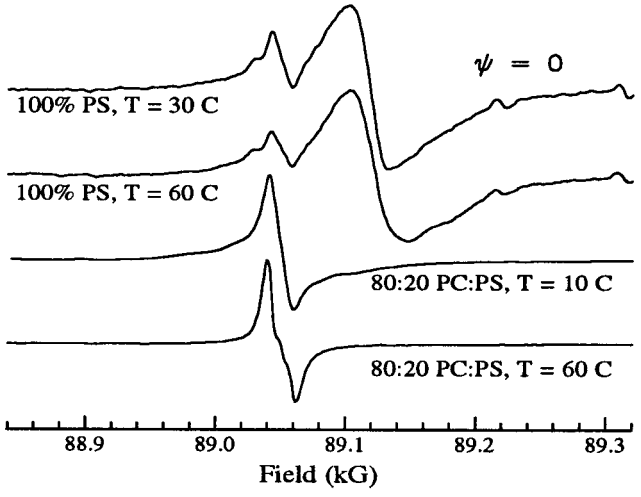

FIGURE 3 A comparison of how the 250-GHz ESR spectra of two of the ISDU-aligned model membranes change when passing from the gel to the liquid-crystal phase, for the $\Psi = 0°$ case. Note the features in the more ordered component of CSL that appear for the L_α phase, which represent the partly resolved A_{yy} component of the hyperfine coupling. The biaxial environment that CSL senses in the DMPS membranes persists in the L_α phase, although for reasons given in the text we present no detailed fit to the data here.

Qualitative lineshape analysis

First, observe the illustrative models of both cholesterol (Shieh et al., 1981) and the CSL molecule shown in Fig. 5. The CSL model was constructed by superimposing two structures determined by x-ray diffraction (Bordeaux et al., 1974; Ishida et al., 1981), consistent with the known configuration of CSL (Marriott et al., 1975). The four fused hydrocarbon rings that form the rigid body of CSL occupy a box of relative dimensions ~1:2:3.6. If we also include the methyl groups sticking out from the broad face of CSL, the extended tail, and the doxyl ring, then the dimensions of CSL are ~1:1.3:4, close to being cylindrically symmetrical. The rigid body of CSL differs only slightly in shape from that of cholesterol, with the most significant difference being the addition of the doxyl ring in place of the hydroxyl group of cholesterol. We consider this further in the Discussion.

To keep track of the orientation of CSL in the bilayers and with respect to the applied static magnetic field $\vec{B}_0$, it is useful to refer to several different coordinate systems (Schneider and Freed, 1989). The principal axes of the diffusion tensor, denoted (x', y', z'), are fixed to the molecular frame of CSL. The principal axes for the g and A tensors are denoted (x''', y''', z'''). For the purpose of a qualitative analysis, we can ignore the small tilt between

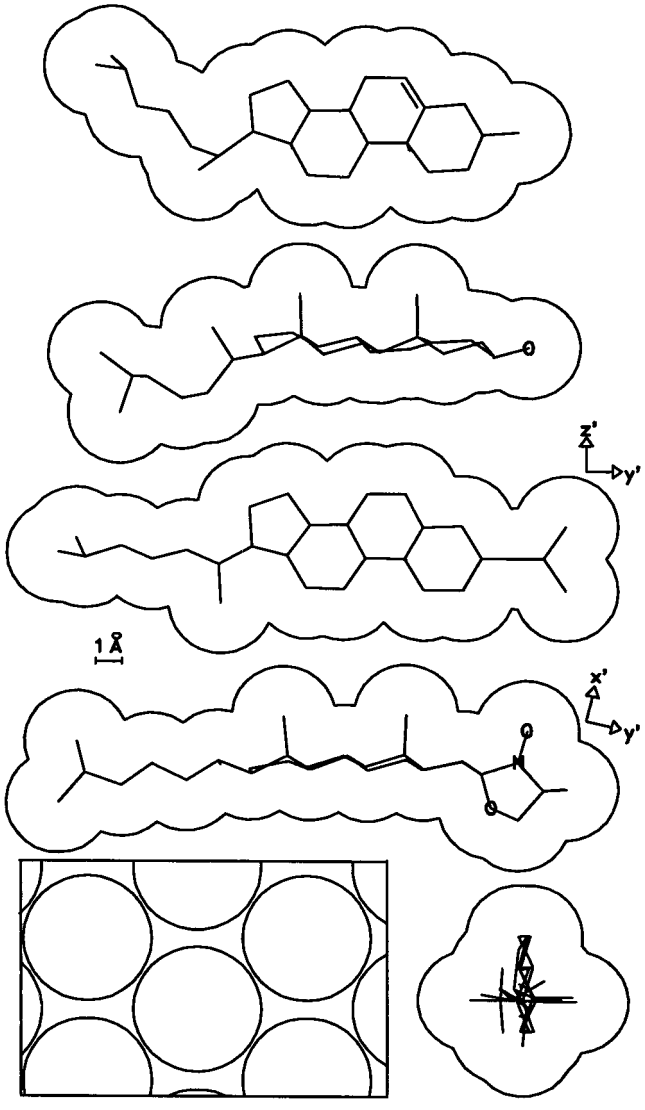

FIGURE 5 A comparison between the structures of cholesterol, shown as the top two structures, and CSL, shown as the middle two structures (see text for details). The contour around the wire frame structures, with a 2.0-Å radius, approximates their van der Waals surfaces. The y' principal diffusion axis of CSL is nearly parallel to the long axis of the molecule. At the bottom of the figure in a box is shown a cross section, normal to the bilayer surface, of the hydrocarbon chain packing in the gel phase of DMPC or DMPS. The circles are the van der Waals surfaces of the lipid hydrocarbon chains. Note that the cross-sectional area of CSL for looking down its long axis (y') occupies a slightly larger area than two of the hydrocarbon chains.

these two coordinate systems. The x' axis lies along the N-O bond, normal to the broad face of the CSL molecule, and the y' axis lies along the long axis of the CSL molecule. The director frame (x'', y'', z'') describes the macroscopically aligned multibilayers. The z'' axis lies parallel to the normal to the bilayer surfaces, $\hat{n}$. The director tilt angle Ψ is the angle between $\vec{B}_0$ and $\hat{n}$.

Cholesterol is known to insert itself into a lipid bilayer with its long axis, y', parallel to the bilayer normal, $\hat{n}$, to minimize steric overlap with the hydrocarbon chains. We denote the orientation with $y' \| \hat{n}$ as the "upright" orientation, as labeled in Fig. 6. As is dramatically shown by the 250-GHz ESR spectra (Fig. 1, *top*), CSL, like cholesterol, orients in an upright position in the aligned and hydrated DMPC bilayers. This confirms the results of previous 9-GHz ESR studies (Shin et al., 1993; Shin and Freed, 1989; Ge et al., 1994b) that, however, required detailed simulations. The most probable orientations of CSL in the DMPC bilayers can be determined from the 250-GHz ESR lineshape by simple inspection, because the lineshape is dominated by the influence of the rhombic g tensor. Specifically, when $\vec{B}_0$ is parallel to the N-O bond ($\vec{B}_0 \| x'$), then $g \approx 2.0088$ and CSL absorbs 250-GHz radiation at a field strength of ~88,920 G. When $\vec{B}_0$ is parallel to the long axis of CSL ($\vec{B}_0 \| y'$), $g \approx 2.0059$ and absorption occurs at ~89,050 G. For $\vec{B}_0$ parallel to the p orbital of the nitrogen atom ($\vec{B}_0 \| z'$), $g \approx 2.0022$ and absorption occurs at ~89,210 G. With this in mind, we can conclude from the position of the single sharp feature in the top spectrum of Fig. 1 that most of the CSL probes in the sample have $y' \| \vec{B}_0$, which in turn is parallel to $\hat{n}$ for $\Psi = 0°$, i.e., the upright orientation. No features in the $\Psi = 0°$ ESR lineshape are observed at higher or lower fields. Thus the probability of finding CSL oriented with either $z' \| \hat{n}$ or $x' \| \hat{n}$, which we will denote as the "sideways" and "facedown" orientations of CSL, respectively (see Fig. 6), must be very small.

Another important observation is available from the $\Psi = 90°$ ESR spectra for which $\vec{B}_0$ lies in the bilayer planes (Fig. 2, *top*). Based on the integrated spectral intensity, a nearly

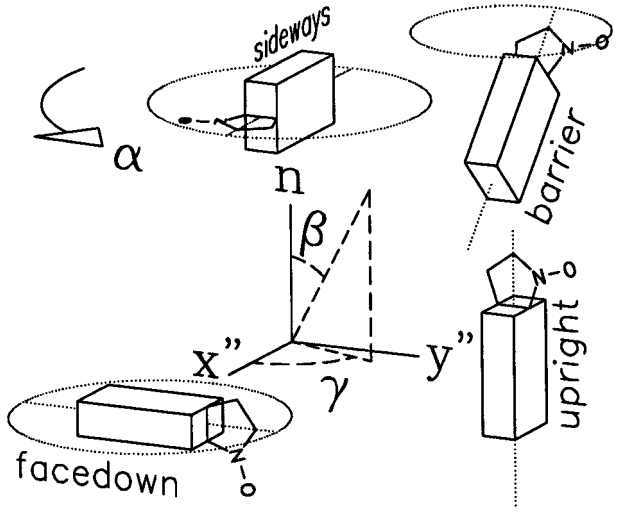

FIGURE 6 Some orientations of CSL with respect to the director frame as a function of the Euler angles β and γ are shown, rotated from an initial orientation of CSL with the diffusion axes aligned with the director axes. The normal to the bilayer surface is given by $\hat{n}$. Because the uniaxial potential is independent of α, we can plot the relative probability of orientation on the two-dimensional surface of β and γ, but it should be kept in mind that each direction in these plots actually represents a collection of orientations with $0 \leq \alpha \leq 2\pi$. This is indicated by the circle traced out by the long axis of CSL as α varies. The orientations described in the text are the sideways orientations, at $(\beta,\gamma) = (0°,0°)$ or $z'' \| \hat{n}$, the upright orientations at (90°,90°) or $y' \| \hat{n}$, the facedown orientations at (90°,0°) or $x' \| \hat{n}$, and the barrier orientations at (45°,90°).

equal superposition of orientations of CSL corresponding to $x' \| \vec{B}_0$ or $z' \| \vec{B}_0$ is observed. Note that the hyperfine coupling with the $I = 1$ ^{14}N nucleus can be easily observed when $z' \| \vec{B}_0$, for which the coupling is at its largest value of ~33 G. The fact that x' or $z' \| \vec{B}_0$ are equally likely orientations confirms that the DMPC bilayers are not macroscopically biaxial. It is not hard to imagine how the packing of the hydrocarbon chains on a hexagonal lattice in the gel phase or a similar regular packing of the phospholipid headgroups could create a microscopically biaxial environment that the rhomboidal CSL could sense (Freed et al., 1994). Such crystal-like order could only be short-range, given the spectral observations. But so far we have presented a static point of view. When we also take into account dynamics, then it is possible for a microscopic biaxiality to strongly influence the ESR lineshapes, even when these environments are only short-range. To the authors' best knowledge, there have been no previous reports of the influence of a local biaxiality on the ordering of cholesterol in either model or biological phospholipid membranes.

In fact, we shall have to invoke local biaxiality to find an adequate interpretation for the ESR spectra associated with CSL in DMPS bilayers. First, note that linear superpositions of the distinctive lineshape of the top and bottom spectra in Figs. 1 and 2 could reasonably describe the rest of the lineshapes for mixtures of DMPC and DMPS. A small amount of the "DMPC-like" component is present in the ESR lineshape for CSL, even in pure DMPS bilayers. Also note that because the $\Psi = 0°$ and 90° ESR spectra for the pure DMPS samples are very different, defects in the sample alignment cannot account for this lineshape unless the defects were uniformly directed in the sample with respect to the ESR spectrometer, and they were undetectable by polarizing microscopy, an unlikely event. Finally, we can ignore the small peaks at 89,030, 89,120, 89,210, and 89,300 G, which are due to a small amount of Mn^{2+} present. We will also ignore in the following fits the small feature at 88,980 G, which is most prominent in the 60:40 DMPC: DMPS spectrum. It is difficult to simulate this feature, but it might be related to forbidden transitions associated with the ^{14}N hyperfine coupling.

The dominant feature of the $\Psi = 0°$ 250-GHz ESR spectrum of CSL in pure DMPS bilayers is a single, broad spectral "line" at $g \approx 2.004$, midway between the lines due to CSL in the upright or sideways orientations (cf. Fig. 6). In a simplified analogy to the "two-site" model (Abragam, 1961), this feature suggests that CSL exchanges its orientations between the upright and sideways orientations at a greater rate than the ESR resonant frequency difference between the two orientations, ~480 MHz. This exchange is described by the parameter R_x, the rotational diffusion rate of CSL about its broad face. When $10^8 < R_x < 10^9$ s^{-1}, the separate g_{yy} and g_{zz} peaks begin to coalesce, as observed in the $\Psi = 0°$ 250-GHz ESR spectrum. However, for the $\Psi = 90°$ spectrum, the sharp line at $g = 2.009$ indicates a population of CSL with $x' \| \vec{B}_0$ that remains in this orientation for times that are long compared to the inverse frequency separation between the different orientations. This suggests that R_y and $R_z \leq 10^7$ s^{-1}.

We illustrate the intuitive model that emerges with Fig. 7. CSL is relatively free to reorient between the upright ($y' \| \hat{n}$) and sideways ($z' \| \hat{n}$) positions by a rotation about its x' axis, but it is hindered from having a facedown orientation ($x' \| \hat{n}$). The effect is one of bringing the long axis of CSL down into the membrane ($y' \| \hat{n} \rightarrow y' \perp \hat{n}$) along the sharpest edge of the body of CSL. This motion is analogous to that of a knife initially held vertically and free to pivot about its broad face so that its edge cuts downward, although with a diffusive type of motion. Rotation of CSL about its y' or z' axes is slow or hindered. This picture also describes the other major feature in the $\Psi = 90°$ ESR spectrum, that of the sharp peak at $g = 2.004$. To see this, note that every CSL, regardless of the orientation of its x' axis in the membrane plane, should have the same kind of ordering and dynamics, because the sample possesses no macroscopic biaxiality. For the $\Psi = 90°$ spectrum, an equal number of CSL molecules will have $x' \perp \vec{B}_0$ in comparison to those with $x' \| \vec{B}_0$, which create the peak at $g = 2.009$. The rapid jumps between $y' \| \hat{n}$ and $z' \| \hat{n}$ for these former molecules then leads to the single feature midway between the upright and sideways orientations, which should be of an intensity similar to that of the feature at $g = 2.009$. This is indeed observed in the $\Psi = 90°$ ESR spectra of CSL in pure DMPS bilayers.

The fact that motions that would rotate the broad face of CSL into its surrounding environment are slow or hindered is consistent with the notion that the interactions of the rigid core of CSL with the surrounding environment strongly influence the ordering and dynamics of this spin probe (Earle et al., 1997). In this case, CSL is still clearly sensing an ordered environment in the DMPS bilayers, although it is less hindered than is the case for the DMPC bilayers.

Using this motional/ordering model for CSL, we can determine what the general features of the 9.1-GHz ESR

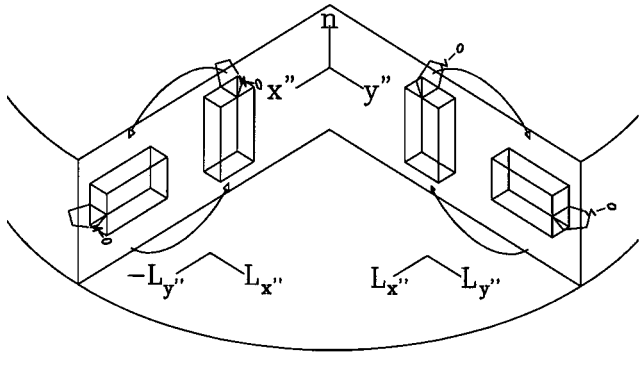

FIGURE 7 A simplified illustration of the motion of CSL in fully hydrated DMPS bilayers. The normal to the bilayer surface is given as $\hat{n}$. The two centermost boxes depict the upright or y-ordered orientation of CSL, the most probable orientation of CSL and cholesterol in DMPC bilayers. In DMPS bilayers, this orientation rapidly exchanges with the sideways, or z-ordered, orientations, as indicated by the arrows. Rotational diffusion of CSL about the y' and z' axis of CSL, or alternatively about $\hat{n}$, are hindered. The different local axis frames, Lx'' and Ly'' for the left-hand pair and the right-hand pair are also shown.

lineshapes should be. The experimental spectra for CSL in 80:20 and in 20:80 mol% DMPC:DMPS bilayers are shown in Fig. 4. They are centered at ~3240 Gauss for the frequency of 9.08 GHz used. For the DMPC-like component of CSL (*top two spectra* of Fig. 4), we expect that for $\Psi = 0°$ we would see features centered at g_{yy} and split by the hyperfine tensor component $A_{yy} \approx 5$ Gauss. For $\Psi = 90°$ we expect features centered at g_{zz} with a splitting of $A_{zz} \approx 33$ Gauss and centered at g_{xx} with a splitting of $A_{xx} \approx 5$ Gauss. For 9.1-GHz ESR lineshapes, however, the shift in going from g_{xx} to g_{yy} or from g_{yy} to g_{zz} is ~5 Gauss, so the g tensor fails to dominate the spectrum, unlike the case at 250 GHz. This is clearly demonstrated in Fig. 8, which shows the positions of the resonant ESR absorptions for the canonical orientations of CSL in a powder simulation at 9.1 and 250 GHz. Thus the extra intensity seen between 3230 and 3240 Gauss in the $\Psi = 90°$, 9.1-GHz ESR spectra is a superposition of absorption from those CSL molecules with $x' \| \vec{B}_0$ and $z' \| \vec{B}_0$. The distinctive features of higher and lower fields seen in the $\Psi = 90°$, 9.1-GHz ESR lineshape, and not in the $\Psi = 0°$ lineshape, are due to the relatively large size of A_{zz}. For 9.1-GHz ESR, the shapes of these features as a function of Ψ are important indicators of the dynamics and ordering of nitroxide spins (Schneider and Freed, 1989). However, we must conclude that there is much poorer orientational resolution at 9.1 GHz than at 250 GHz.

For the DMPS-like component of CSL, the rapid rotational diffusion between the upright and sideways orientations of CSL will partly average the g and A tensors, resulting in a broad feature with an average $A \approx 20$ Gauss for the $\Psi = 0°$, 9.1-GHz ESR spectra. A similar feature will exist for the $\Psi = 90°$ spectra, along with the sharper features centered at g_{xx} with a splitting of $A_{xx} \approx 5$ Gauss due to those CSLs constrained to keep $x' \| \vec{B}_0$. The bottom two 9.1-GHz ESR lineshapes of Fig. 4 are in qualitative agreement with these observations. The $\Psi = 0°$ spectrum does show intensity, suggesting a range of splittings between 10 and 30 Gauss, whereas the $\Psi = 90°$ spectrum could be represented by a superposition of these same broad features with extra intensity at ~3230 Gauss. However, there is a significant overlap between these different features, and thus significant loss of resolution in the 9.1-GHz spectra as compared with the 250-GHz spectra. This reduced resolution implies considerable ambiguity, i.e., different sets of motional/ordering parameters in addition to the ones that fit the 250-GHz ESR spectra may also adequately fit the 9.1-GHz spectra in a least-squares sense. If we had only the 9.1-GHz ESR spectra and no further physical insights into the system, then we would have a number of motional/ordering models of CSL in DMPS from which to choose. The much greater orientational resolution of the 250-GHz ESR spectra is clearly very significant in determining a unique model for CSL in the DMPS bilayers.

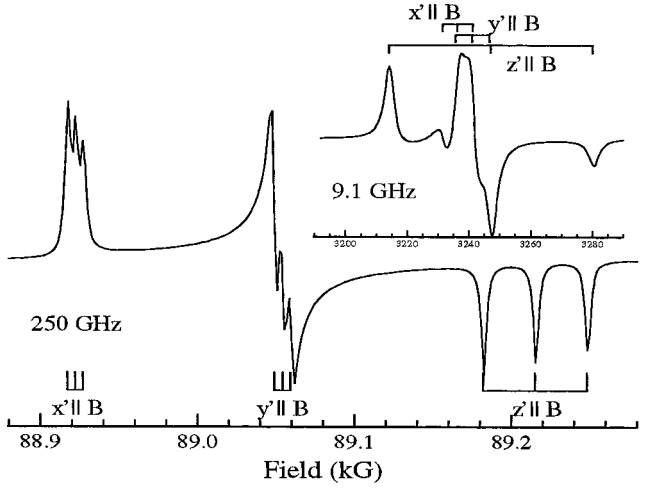

FIGURE 8 A powder simulation of CSL at 9.1 and 250 GHz. The connected vertical dashes represent the fields where CSL will absorb when its x', y', or z' axes are parallel to $\vec{B}_0$. Whereas at 250 GHz these occur at well-separated spectral regions, at 9.1 GHz there is considerable overlap.

Quantitative lineshape analysis

In this section we convert the intuitive motional/ordering model described in the last section into a quantitative model for a least-squares lineshape analysis (Budil et al., 1996). CSL is termed a "y-ordered probe" in lipid bilayers because it is a nearly cylindrically symmetrical probe whose principal axes of rotational diffusion in general lie parallel and perpendicular to y' (see Fig. 5). For a least-squares fit, if the magnetic tensor parameters are used in a permuted order with g_{zz}, g_{xx}, and g_{yy} entered in place of g_{xx}, g_{yy}, and g_{zz}, and similarly for A, the result is that the long axis of CSL is now aligned with the principal diffusion axis. That is, we would have that $z''' \| x'$, $x''' \| y'$, and $y''' \| z'$. This is particularly advantageous when there is axial symmetry about the y' axis in the rotational diffusion tensor. This has proved useful in many cases (Earle et al., 1997; Ge et al., 1994b; Shin et al., 1993). However, the model outlined in the last section for CSL in the DMPS bilayers suggests that using a "y-ordering" for CSL is less helpful when discussing CSL in the DMPS bilayers. In our present discussion, we do not permute the magnetic tensor elements for the least-squares fits that follow. In the absence of any diffusion tilt, this is equivalent to setting $x''' \| x'$, $y''' \| y'$, and $z''' \| z'$. This is consistent with our quantitative discussion in the previous section. The effects of magnetic axis permutation on the ordering parameters (cf. Eq. 1 below) are discussed in the Appendix.

To interpret the potential parameters, we show in Fig. 6 the orientations of CSL with respect to the laboratory-fixed director frame as a function of β and γ. Recall that the Euler angles (α, β, γ) are the angles that transform from the director frame to the diffusion frame of CSL (Schneider and Freed, 1989). The Euler angle α is the final rotation of CSL about the $\hat{n}$ axis, and it is unnecessary for the uniaxial case.

The orientation-dependent potential used in the fits is given by the form (Schneider and Freed, 1989)

$$-U(\beta, \gamma) = c_{20}(3\cos^2\beta - 1)/2 + c_{22}(3/2)^{1/2}\sin^2\beta\cos 2\gamma + c_{40}(35\cos^4\beta - 30\cos^2\beta + 3)/8 + c_{42}(5/8)^{1/2}(7\cos^2\beta - 1)\sin^2\beta\cos 2\gamma + c_{44}(35/32)^{1/2}\sin^4\beta\cos 4\gamma \quad (1)$$

where the potential parameters c_{20}, c_{22}, c_{40}, c_{42}, and c_{44} are given in units of kT. Equation 1 is an expansion in Wigner rotation matrix elements, which in the present uniaxial case reduces to unnormalized spherical harmonics. The relative or unnormalized probability of CSL having an orientation in the infinitesimal range $\beta \pm \Delta\beta$ and $\gamma \pm \Delta\gamma$, for any α, is given by $\exp(-U(\beta,\gamma)/kT)\sin\beta\,\Delta\beta\,\Delta\gamma$. Given a set of potential parameters, we can plot this relative probability as a function of the spherical coordinates (β, γ) and, by comparison with Fig. 6, identify the most and least probable orientations of CSL.

The result of a least-squares fit to the 80:20 mol% DMPC:DMPS model membrane using only the c_{20} and c_{22} terms in the potential and the magnetic tensor parameters in Table 2 (cf. below) is shown in Fig. 9 *A*, with the motional and ordering parameters given in column A of Table 3. The corresponding potential is plotted as Fig. 10 *A*. It shows a preference for having $y' \| \hat{n}$. There is also a weak "rhombic distortion" such that $z' \| \hat{n}$ is slightly preferred over having $x' \| \hat{n}$. Note that the potential allows a high enough probability of finding CSL with $y' \perp \hat{n}$ to account for the small peak at g_{yy} in the $\Psi = 90°$ spectrum. It is also found that the rotational diffusion rates are slow, with R_y and $R_z \approx 10^7$ s^{-1}. The rate for R_x is significantly slower. A slower motion may improve the fit slightly, but the basis set required for convergence of the 250-GHz ESR lineshapes becomes impractically large: values of $R < 10^5$ s^{-1} correspond to L_{max}, K_{max}, and $M_{max} \geq 50$ (Schneider and Freed, 1989). In contrast, a typical basis set size for 9-GHz ESR lineshapes requires L_{max}, K_{max}, and $M_{max} \leq 12$.

For slow motions, the 250-GHz ESR lineshape is sensitive to a tilt between the diffusion axes and the magnetic axes of CSL. Such a tilt could arise from a small (13°) tilt of the N-O bond with respect to the broad face of CSL (Schneider and Freed, 1989) or from a tilt of the hydrocarbon chains with respect to the bilayer normal (Marsh, 1988; Sun et al., 1994). However, the least-squares fits showed a preference for a tilt angle of 0°. But there is no significant change when the value of the tilt is fixed at 13° in the fitting process, as shown in Fig. 9 *B*, with the least-squares parameters given in Table 3, column B.

TABLE 2 Magnetic tensor parameters determined from the 250-GHz ESR lineshape of CSL in the DMPC-rich bilayers

$g_{xx} = 2.00871$	$g_{yy} = 2.00573$	$g_{zz} = 2.00210$
$A_{xx} = 4.9$	$A_{yy} = 5.5$	$A_{zz} = 33.1$

Within experimental uncertainty, these results are in agreement with previous results obtained at 9 GHz (Kar et al., 1985; Ge et al., 1994a).

We determined the magnetic tensor parameters g and A from the 250-GHz ESR spectrum of CSL in DMPC. They are given in Table 2. The sweep field was calibrated using TEMPONE frozen in a water-glycerol mixture at −100°C (Budil et al., 1989). For the remaining fits, the 250-GHz ESR lineshapes are much broader, and so as a reasonable approximation we fixed the magnetic tensor parameters at the values in Table 2 and varied only the motional and ordering parameters.

The spectra from the pure DMPS bilayers show a small "DMPC-like" component as noted above. For convenience in the simulations we shall ignore this component initially. After we determine a satisfactory model for fitting the DMPS component, we then determine the admixture of "DMPC-like" to "DMPS-like" components for the series shown in Figs. 1 and 2. This procedure is justified a posteriori by the finding (cf. below) the the spectra from the pure DMPS bilayers are composed of >90% of the "DMPS-like" component.

The best fit for CSL in the pure DMPS bilayers achieved by varying only the potential terms c_{20} and c_{22} and the full rotational diffusion tensor is shown as Fig. 9 *C*. From the shape of the potential shown as Fig. 10 *C*, it can be seen that both the sideways and upright orientations are now favored, consistent with the model of Fig. 7. The addition of the potential terms c_{40}, c_{42}, and c_{44} yields a slightly better fit (Fig. 9 *D*), resulting from the addition of a barrier to the rotation of CSL about its broad face (the x' axis) between the upright and sideways orientations (Fig. 10 *D*). A fit using a very high barrier to the reorientation of CSL was also tried (Fig. 9 *E*, with the potential shown as Fig. 10 *E*), but it did not significantly improve the fit. We also attempted to improve the fits by modeling the slow tumbling rate of CSL about its long axis, using anisotropic viscosity (Schneider and Freed, 1989), which incorporates an independent rotational diffusion of CSL about the bilayer normal, $R_\parallel^{av}$, and perpendicular to it, $R_\perp^{av}$. The result is shown as Fig. 9 *F*. However, it is clear that the models considered fail to incorporate some aspect of the dynamics/ordering of CSL in the bilayers.

For the above fits, the greatest discrepancy occurs in the range of 88,940–89,100 G for the $\Psi = 90°$, 250-GHz ESR spectrum. Examination of the motional model suggested by Fig. 7 gives a possible explanation: each CSL, which includes those to the right and to the left in Fig. 7, is constrained by the lipids that surround it, so that interconversion of a CSL between the two orientations to the left (or right) of Fig. 7 is relatively unhindered, but interconversion between an orientation on the left to one on the right is hindered. Of course, Fig. 7 illustrates only two "orientational pairs," whereas there are CSLs at every angle with respect to the static magnetic field, $\vec{B}_0$, for the $\Psi = 90°$ case, which would experience a similar hinderance. Simple considerations, which are quantitatively verified below, indicate that this will improve the fit.

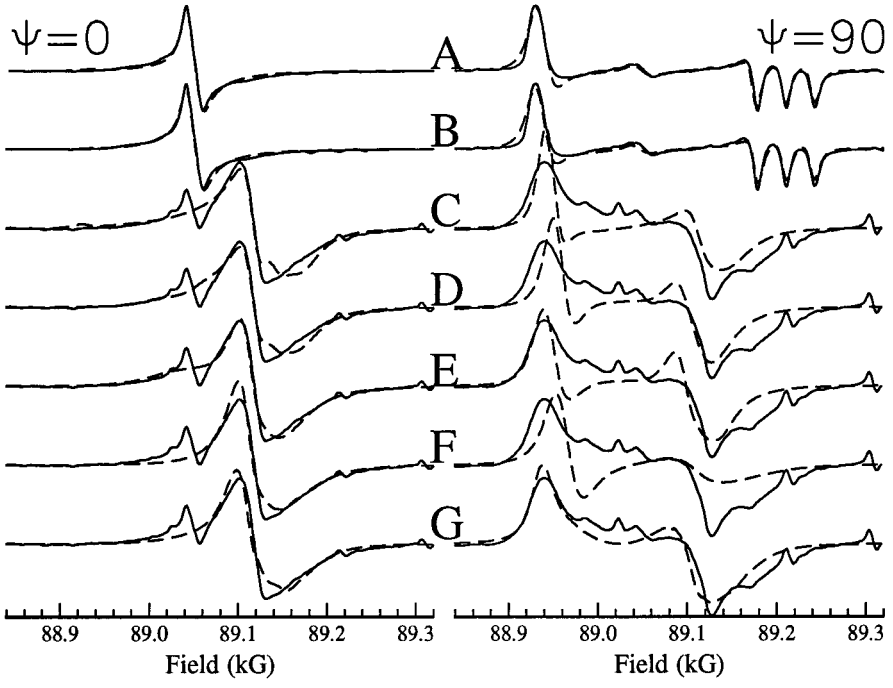

FIGURE 9 The results of simultaneous fits to the $\Psi = 0°$ and $\Psi = 90°$ ESR spectra of CSL in the gel phase of 80:20 mol% DMPC: DMPS are shown in *A* and *B*, and those from pure DMPS are shown in *C–G*, using different models for the ordering and dynamics as described in the text. The parameters from these fits are given in Table 3.

A biaxial potential correctly describes the motional/ordering model just discussed, but it results in a more complicated form of Eq. 1 (Freed et al., 1994; Berggren, 1995). However, because the above fits suggest that reorientation about the bilayer normal $\hat{n}$ is nearly frozen out on the 250-GHz ESR time scale, we can use an alternative version of the model that has the advantage of being computationally tractable. Specifically, we assume that a CSL is constrained by a potential such that its x' axis remains nearly parallel to a local director axis, $\hat{n}_L$, which we will find is equivalent to the Lx'' (e.g., the local axis systems are shown in Fig. 7 for both the left- and right-hand pairs of orientations). Because the sample is not macroscopically biaxial, we expect the local directors to be uniformly distributed within the bilayer plane. Thus the ESR lineshape consists of a sum of ESR spectra, one for each $\hat{n}_L$ in the membrane plane. A simple sum is reasonable because exchange between CSLs with different local directors is taken as very slow on the 250-GHz ESR time scale. We now use a uniaxial potential with respect to the $\hat{n}_L$, such that rotations of CSL about $\hat{n}_L$ are allowed, but rotations of CSL that tilt the N-O bond with respect to $\hat{n}_L$ are restricted (cf. Fig. 10 *G*).

A more general version of this distribution-of-directors kind of motion has been discussed previously (Meirovitch et al., 1982). It is implemented as follows. Referring to Fig. 11, the sample possesses a macroscopic director axis $\hat{n}$, about which there is a distribution of local director axes $\hat{n}_L$ whose orientation relative to $\hat{n}$ is given by the polar angles (ξ,ζ). For generality, each orientation of $\hat{n}_L$ is weighted by a probability factor of the form $\exp(-V(\xi,\zeta))\sin\xi\,d\xi\,d\zeta$. For our model we can choose $V = -dc_{20}\cos^2\xi$, where dc_{20} is the only new parameter in the fit. The ESR spectrum for a given

TABLE 3 Motional and ordering parameters from least-squares fits

Parameter/model	A	B	C	D	E	F	G
β_D	0	13	0	0	0	0	0
R_x	$2 \cdot 10^5$	$2 \cdot 10^5$	$8 \cdot 10^8$	$2 \cdot 10^9$	$3 \cdot 10^9$	$5 \cdot 10^6$	$1 \cdot 10^9$
R_y	$7 \cdot 10^6$	$1 \cdot 10^7$	$9 \cdot 10^5$	$1 \cdot 10^5$	$5 \cdot 10^7$	$5 \cdot 10^6$	$6 \cdot 10^7$
R_z	$1 \cdot 10^7$	$2 \cdot 10^7$	$1 \cdot 10^7$	$5 \cdot 10^6$	$1 \cdot 10^5$	$5 \cdot 10^6$	$3 \cdot 10^6$
$R_\parallel^{av}$	—	—	—	—	—	$1 \cdot 10^5$	—
$R_\perp^{av}$	—	—	—	—	—	$5 \cdot 10^8$	—
c_{20}	−0.81	−0.36	1.40	2.00	0.90	2.0	−5.16
c_{22}	−1.47	−2.00	−1.17	−1.50	−0.84	−2.6	2.13
c_{40}	—	—	—	0.0	0.89	—	0.0
c_{42}	—	—	—	1.0	1.15	—	−2.28
c_{44}	—	—	—	0.0	0.0	—	0.0
dc_{20}	—	—	—	—	—	—	−20.0

The letters A–G labeling the columns refer to the ESR spectra in Fig. 9. Rotational diffusion rates are given in units of s^{-1}, and the potential parameters are in units of kT.

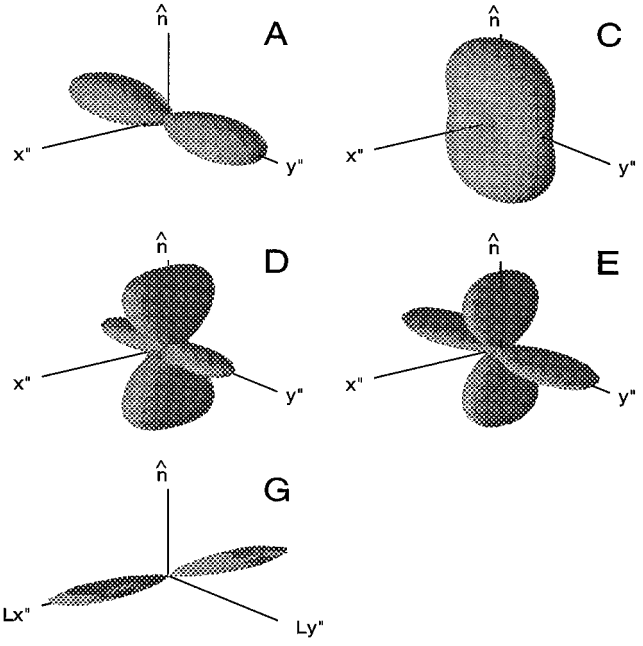

FIGURE 10 Plots of the unnormalized probability distribution, $\exp(-U(\beta,\gamma)/kT)$, correspond to the fits whose parameters are given in columns A, C, D, E, and G of Table 3. $\hat{n}$ is the normal to the bilayer plane. The peaks along the y'' axis in the probability distribution shown in *A* indicate that the "upright" orientation of CSL (i.e. $y' \| \hat{n}$, cf. capiton to Fig. 6) is favored in the DMPC-rich bilayers. The distributions labeled as *C*, *D*, and *E* show that the "sideways" orientation of CSL, as indicated by the peaks along the z'' axis (parallel to $\hat{n}$), is also a favored orientation for CSL in the DMPS-rich bilayers. The distribution G keeps the N-O bond of CSL aligned along the local director axis Lx'', which is constrained to lie parallel to the bilayer plane because the local director distribution parameter dc_{20} was found to be large and negative.

Ψ is then the sum over the spectra due to all possible orientations of $\hat{n}_L$,

$$\tilde{I}(B, \Psi) = \int_0^{2\pi} d\zeta \int_0^{\pi} \sin \xi \, d\xi \, I(B, \Psi, \xi, \zeta) e^{-V(\xi,\zeta)}$$

in which $I(B,\Psi,\xi,\zeta)$ is the ESR spectrum for a given $\hat{n}_L$. This can be evaluated by transforming to a coordinate system by using an effective overall director tilt Ψ_{eff} and an azimuthal rotation angle φ, as detailed in Fig. 11. It can be shown that

$$\cos \xi = \sin \Psi \sin \Psi_{eff} \cos \varphi + \cos \Psi \cos \Psi_{eff}$$

$$\tan \zeta = \frac{\sin \Psi_{eff} \sin \varphi}{\cos \Psi \sin \Psi_{eff} \cos \varphi - \sin \Psi \cos \Psi_{eff}}$$

and the double integral becomes

$$\tilde{I}(B, \Psi) = \int_0^{\pi} I(B, \Psi_{eff}) \left(\int_0^{2\pi} e^{-V(\Psi, \Psi_{eff}, \varphi)} d\varphi \right) \sin \Psi_{eff} \, d\Psi_{eff}$$

The integration is now performed in a manner similar to that of a microscopic order with macroscopic disorder (MOMD)-type calculation (Budil et al., 1996), except that

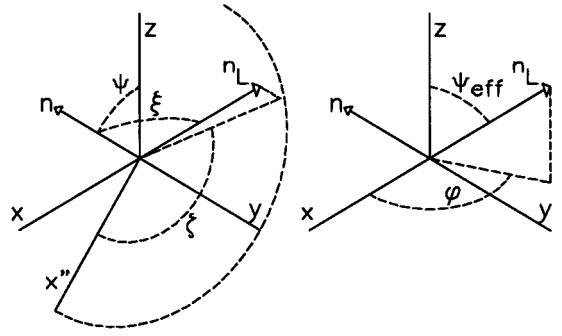

FIGURE 11 (*Left*) Diagram of the relation between the lab frame (x, y, z) and the director frame (x'', y'', $\hat{n}$) with $y'' \| y$, where Ψ is the director tilt angle and $\hat{n}$ is normal to the bilayer surface. The dashed circle represents the disk-shaped sample. The local director axis, $\hat{n}_L$, is at the polar angles (ξ,ζ) with respect to $\hat{n}$. (*Right*) Relation between $\hat{n}_L$ and the laboratory frame expressed in terms of the polar angles (Ψ_{eff},φ). They can be written as functions of ξ,ζ and Ψ. The angle Ψ is set by the experimenter, but the local director axes $\hat{n}_L$ are distributed over all values of (ξ,ζ), with some probability distribution given by $[\exp - V(\xi,\zeta)] \sin \xi \, d\xi \, d\zeta$.

the angle Ψ_{eff} varies from 0 to π, and each spectrum is weighted by the exponential in V over the potential term. (For the case of true MOMD-like disorder, for example, in the application of this model to a vesicle dispersion, we must add a third integral over Ψ. The resulting expression using the $\cos^2\xi$ form for the local director potential, however, can be shown to reduce to the standard integrand for a MOMD-type spectrum, i.e., the double integral of $\exp(-V)$ over Ψ and φ has no Ψ_{eff} dependence. Thus, for the motional model we are employing, a macroscopically aligned sample is essential.)

The best fit obtained with this model is shown as Fig. 9 *G*. It gives a satisfactory representation of all of the major features of the 250-GHz ESR spectra for both $\Psi = 0°$ and 90°, including the slow roll-off in intensity above the g_{xx} peak. The large, negative value for dc_{20} means that the local directors are uniformly distributed in the plane perpendicular to $\hat{n}$, which is the expected macroscopic uniaxial behavior that we have already discussed.

To fit the 250-GHz ESR lineshapes for the remaining compositions of DMPC/DMPS, we fixed both the magnetic and motional/ordering parameters of the DMPC-like and DMPS-like components of CSL, and used the multicomponent fitting ability of our programs to determine the weighting of the two components necessary to best fit each lineshape (Budil et al., 1996). To determine if a detectable exchange rate between the two different motional/ordering components of CSL could be observed, we also allowed the linewidth parameter of the DMPC-like component of CSL to vary as a function of bilayer composition (see Table 1). Some increase in the linewidth was observed for the midrange of membrane compositions, which might imply some exchange, but this is not unequivocal. The small percentage of the DMPC-like motional/ordering component of CSL in the pure DMPS bilayers is accurately measured, because of the much smaller linewidth of the DMPC-like component.

DISCUSSION

To summarize: CSL in the fully hydrated gel phase of a DMPC-rich bilayer is oriented with the long axis of the molecule, y', parallel to the normal to the bilayer, $\hat{n}$, as is the case for cholesterol. CSL in the gel phase of a fully hydrated DMPS bilayer, however, reorients rapidly about its x' axis. This motion can be visualized as CSL cutting into the hydrocarbon layer along its (slightly) sharper edge, as in Fig. 7. All orientations of x' in the bilayer plane are equally probable, and rotational diffusion about y' and z' is relatively slow. What interactions occur in the DMPS bilayers that are so different from those in the DMPC bilayers, such that CSL finds itself sensing a locally biaxial environment?

ESR studies of CSL at 9 GHz in ISDU-aligned DPPC bilayers below 0°C (Kar et al., 1985; Ge et al., 1994a) have demonstrated that the N-O group of CSL participates in hydrogen bonding. Moreover, the value of A_{zz} for CSL given in Table 3 for the DMPC-rich bilayers shows that the doxyl ring is in a relatively hydrophilic environment (Earle et al., 1993; Ge and Freed, 1998) and is thus oriented with the doxyl ring near the bilayer surface. Thus the doxyl ring plays a role somewhat similar to that of the hydrogen-bonding hydroxyl group of cholesterol, which also participates in hydrogen bonding at the bilayer surface, as discussed in more detail by Ge et al. (1994a).

CSL in a phospholipid bilayer is usually observed to have an axially symmetrical rotational diffusion tensor with the faster diffusional rate, R_y, being about the long axis of CSL, and with R_x,$R_z \approx 1/5$ of R_y (Earle et al., 1993, 1997). In the L_α phase we expect that $10^8 \leq R_y \leq 10^9\ s^{-1}$ (Ge et al., 1994b), whereas in the gel phase the motions are slower, $R_y \leq 10^7\ s^{-1}$ (Meirovitch and Freed, 1980). This is in agreement with what was found for CSL in the DMPC bilayers. However, in pure DMPS bilayers for CSL, we find that $R_x \approx 10^9\ s^{-1}$, a rapid rate. In fact, it is much greater than what is expected for the rotational diffusion rates for the hydrocarbon chains in the gel phase, $2 \times 10^6\ s^{-1}$ about $\hat{n}$ and $2 \times 10^5\ s^{-1}$ perpendicular to $\hat{n}$ (Yeagle, 1991). It seems reasonable to conclude that CSL is reorienting in a "stable void" when in the DMPS bilayer.

Because no large broadening of the DMPC-like component is observed in DMPS, we conclude that exchange between the DMPC-like and DMPS-like components of CSL is slow on the 250-GHz ESR time scale, and therefore the void in which CSL orients is stable for at least microseconds. Furthermore, x-ray diffraction data on DMPS vesicles in the gel phase show that the hydrocarbon chains pack on a hexagonal lattice, with no indication of a significant population of voids (Hauser and Shipley, 1983). We conclude that the insertion of the cholesterol-like CSL into the DMPS bilayers creates these voids.

No unusual ordering of CSL was found for the L_α phase of mixed PC/PS multibilayers with unsaturated hydrocarbon (Ge et al., 1994b), or for a fluorescent cholesterol analog in bovine PS vesicles, which also contain unsaturated lipids (Yeagle et al., 1990). This could imply that either saturated hydrocarbon chains, or a gel-like phase, including a condensed phase beneath a positively charged membrane-associated protein, is important in creating these voids. Furthermore, for the latter case, one should consider the differences in morphology between oriented membranes and vesicles (Ge and Freed, 1998). Dual "upright" and "sideways" orientations in fully saturated PC bilayers have been observed for both a long, rod-shaped hydrophobic fluorescent probe (Mitchell and Litman, 1998) and a cigar-shaped nitroxide probe (Meirovitch, 1983).

We now consider what difference between DMPC and DMPS might lead to the unusual ordering of CSL observed in DMPS. Aggregation (but not actual phase separation) of DMPS in DMPC, characteristic of a nonideal solution, probably does occur (Hinderliter et al., 1994). Phase separation can be induced by a low pH in which PS becomes protonated (Tokutomi et al., 1980), but in our samples the PS headgroups are buffered by Na^+, and the ISDU solutions before ultracentrifugation had a pH of ~7.8. However, aggregration of DMPS is a reasonable explanation of the sudden increase in the DMPS-like motional/ordering component of CSL when the molar ratio of DMPS in the bilayers rises above ~1/3. This suggests that CSL prefers the DMPS aggregrates. Although the misciblity of cholesterol is higher in PC than in PS bilayers (Wachtel et al., 1991), for low concentrations of cholesterol (and very probably CSL), it prefers to interact with hydrocarbon chains in an extended conformation (Ipsen et al., 1987). As discussed before, this conformation is more likely for DMPS than for DMPC, which could represent the driving force for the partitioning of CSL into the DMPS aggregrates.

It could be argued that the difference in the hydrocarbon chain tilt with respect to $\hat{n}$ of 20–30° for the gel phase of DMPC (Sun et al., 1994) versus 0° for the gel phase of DMPS (Hauser and Shipley, 1983) leads to "void formation" at the interface between the DMPC/DMPS aggregates. However, this contradicts the fact that the voids are observed even when no DMPC is present. In fact, if hydrocarbon chain packing efficiency were the sole cause of the void formation, then the following line of reasoning might be applied: it is known from studies of crystallized PC lipids that chain tilts or lateral offsets of the hydrocarbon chains, leading to disorder or small void formation at the bottom of the hydrocarbon chains, often occur to accommodate the packing of the relatively large PC headgroups (Marsh, 1988). In contrast, the PS headgroup is similar in size to the two hydrocarbon chains, leading to a more efficient packing and a stabilization of the gel phase of DMPS as compared to DMPC (T_m = 45°C and 23°C, respectively; Marsh, 1988). This occurs despite the fact that a charged phospholipid tends to destabilize the gel phase (Boggs, 1987). This line of reasoning suggests that significant voids should be expected in DMPC instead of DMPS, which is inconsistent with our results. We can also rule out the possibility that aggregation of CSL leads to void formation in DMPS, because this would result in an observable spin-spin broadening of the ESR lineshapes.

We do not believe that the voids in DMPS are a consequence of the dehydration of the bilayers during the ISDU alignment process (Takahashi et al., 1997). It is difficult to see how small defects, on the order of the size of CSL, could survive rehydration and even annealing into the L_α phase. If larger, stable pores were to form, they would create a distribution of local bilayer normals uniform about the macroscopic director axis of the sample, leading to a MOMD type of ESR lineshape (cf. Fig. 12). The addition of a MOMD lineshape will create features independent of Ψ, and such features are not observed in the spectra of Figs. 1 and 2.

We also rule out the possibility that the DMPS-rich bilayers are distorted by the high magnetic field. Bilayers tend to orient with $\hat{n} \perp \vec{B}_0$ because of the diamagnetic anisotropy of the hydrocarbon chains. However, only certain vesicle dispersions of specific mixtures of lipids, none of which include any PS lipids, have been shown to have large effects (Speyer et al., 1987). Multilaminar vesicles are also less susceptible than unilamilar vesicles (Brumm et al., 1992). These facts suggest that the multilamilar ISDU-aligned samples should be more resistant to the effects of the high magnetic field. If the magnetic field were to cause local distortions of the bilayers, it would create a distribution of directors, and thus of tilt angles Ψ, in the sample. Fig. 12 shows how the 250-GHz spectrum of the DMPC-like component of CSL changes with the tilt angle. No such weighted sum of these spectra could account for the sharp peak at $g = 2.004$. Similarly, the absence of any features at the g_{xx} region for the $\Psi = 0°$ spectrum places a strict upper limit on the presence of any bilayers with locally larger values of Ψ. Furthermore, any significant realignment of the bilayers is expected to lead to disordered regions, given the sample sensitivity, e.g., to thermal changes. However, sample immersion in the 8.9-T field for 10 or more hours did not lead to any defects observable by microscopy. Note that if the magnetic field had created a reversible distortion (Meirovitch and Freed, 1980), then it should lead to a macroscopic biaxial environment, and in our fits we found no evidence for this. Finally, note that the 9-GHz ESR lineshapes are consistent with the proposed motional/ordering model for CSL in DMPS, where magnetic field-induced effects, which depend upon $|\vec{B}_0|^2$, are a factor of ~770 times lower. This would be difficult to verify by using a detailed fitting because of the greatly reduced orientational resolution for 9-GHz ESR spectra. Furthermore, the assumption that reorientational diffusion of CSL about $\hat{n}$ is "frozen out" is probably no longer valid on the longer 9-GHz time scale (Earle et al., 1993, 1997). Thus a much more complicated dynamical, biaxial calculation would be required. The weight of the above evidence suggests, however, that magnetic field effects are not responsible for the creation of the voids in DMPS.

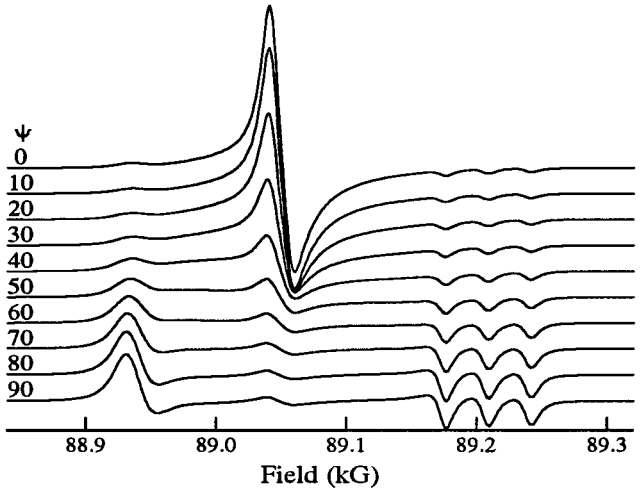

FIGURE 12 A simulation of the DMPC-like component of CSL at 250 GHz, as a function of the director tilt angle Ψ, using the parameters in Table 3, column A.

The only difference between DMPC and DMPS is in their headgroups. The PS headgroups are known to interact with one another more strongly, and with potentially more hydrogen bonding sites, than that of PC (Boggs, 1987). These electrostatic interactions are enhanced by the negative charge on PS, which is not shielded by monovalent cations (except for the case of Li^+; Cascales and de la Torre, 1997). As a result, the PS headgroups in a pure PS bilayer are more rigid than for the PC headgroups in a pure PC bilayer (Kohler and Klein, 1977; Campbell et al., 1979). In fact, the addition of Li^+ to DMPS bilayers raises T_m to 90°C, whereas the hydrocarbon chain packing becomes tight enough so that a pseudocrystalline phase has been identified below 15°C (Hauser and Shipley, 1983). The headgroups adopt packing schemes that minimize their total free energy, such that the long axis of PC tries to tilt perpendicular to $\hat{n}$, but that of PS lies parallel to $\hat{n}$ (Sanson et al., 1995). In this packing scheme, the dipole moments of both PC and of the zwitterionic serine group of PS lie perpendicular to $\hat{n}$. Although no long-range order has been observed for the headgroups in hydrated bilayers, molecular dynamics simulations indicate that dipolar interactions can lead to domains of ordered headgroups (Schneider and Keller, 1997). In the simulated packing, the net dipole moments of the headgroups form an antiferroelectric phase on a 2D hexagonal lattice (Kittel, 1976). This arrangement is strongly biaxial in character, and thus we suggest that maintaining this PS headgroup packing arrangement is what forces the entropically unfavorable void formation for CSL in the DMPS bilayers. This interpretation seems consistent with the observation that stronger headgroup interactions will lower the miscibility of cholesterol in both the L_α and, to a greater extent, the gel phases of pure PS bilayers (McMullen and McElhaney, 1997).

That cholesterol may lead to void formation in the gel phase, and possibly also the L_α phase, of DMPS has implications for protein/lipid interactions, as discussed in the Introduction. It is of relevance to consider the effects of cholesterol in the microdomains of PS below a positively charged, membrane-associated protein such as PKC. The

~30 mol% solubility limit of cholesterol in PS-rich bilayers (Wachtel et al., 1991) seems high enough to have a significant impact on the characteristics of these domains. The formation of voids would be expected to dilute the degree of negative charge that can accumulate below a protein to an even greater degree than simple packing and solubility considerations would suggest. However, the voids also represent stable pockets into which a myristate group could insert, and thus the cholesterol/PS void could decrease the free energy of binding of myristoylated proteins by increasing the solubility of the myristate group in the bilayers.

CONCLUSION

In summary: the use of FIR ESR spectra at 250 GHz, which provides very good orientational resolution, has made possible an unambiguous determination of a local biaxial environment sensed by the nitroxide-labeled cholesterol analog CSL in the hydrated bilayers of the gel phase of DMPS. The locally biaxial environment provides a void that allows CSL to cut into the hydrocarbon chain region of the bilayers by reorienting about its broad face. The voids are postulated to exist for DMPS but not for DMPC, because of the stronger interactions between the PS headgroups, which causes the PS lipids to form aggregates that pack inefficiently around CSL to maintain a local, biaxial headgroup packing arrangement.

APPENDIX: THE ORIENTATIONAL POTENTIAL

In this section we will show how to convert between orientational potentials with and without using y-ordering in a fit (i.e., permuting the magnetic tensor elements in the lineshape programs to achieve $z'''\|x'$, $x'''\|y'$, and $y'''\|z'$). The orientational potential given by Eq. 1 has been discussed in several places and has recently been reviewed (Freed et al., 1994). A complete expansion of the potential is given in terms of generalized spherical harmonics as

$$U(\alpha, \beta, \gamma) = \sum_{L,M,K} c^{L}_{MK} \mathcal{D}^{L}_{MK}(\alpha, \beta, \gamma)$$

for which U must be a real function. If we assume that the CSL molecule has approximately D_2 symmetry, i.e., the rectangular parallelepipid form shown in Fig. 6, then the expansion can be simplified to

$$U(\alpha, \beta, \gamma) = \sum_{L,M,\bar{K}} c^{L}_{M\bar{K}} (\mathcal{D}^{L}_{M,\bar{K}}(\alpha, \beta, \gamma) + \mathcal{D}^{L}_{M,-\bar{K}}(\alpha, \beta, \gamma))$$

where $\bar{K} = 0,2,4,\ldots$. In a uniaxial environment, the potential should be independent of α, and thus we have

$$U(\beta, \gamma) = \sum_{L,\bar{K}} c_{L,\bar{K}} (\mathcal{D}^{L}_{0,\bar{K}}(\beta, \gamma) + \mathcal{D}^{L}_{0,-\bar{K}}(\beta, \gamma))$$

The expansion in a liquid-crystalline medium is usually taken over L-even. Although this is not strictly true in a bilayer composed of chiral phospholipids unless the probe molecule truly has D_2 symmetry, it serves as a useful approximation that is commonly used (Schneider and Freed, 1989). As a practical matter, only the lowest order terms in the expansion are utilized, i.e., $L = 2$ or 4. This leaves the following nonzero coefficients in the expansion: the two $L = 2$ terms, c_{20} and c_{22}, and the three $L = 4$ terms, c_{40}, c_{42}, and c_{44}. Note that we are using the notation $c_{L,\bar{K}} \equiv c^{L}_{0,\bar{K}}$ for $\bar{K} \neq 0$, and $c_{L0} \equiv c^{L}_{0,0}/2$.

A further property is that c_{20} and c_{22} are the components of an irreducible tensor of second rank, and the c_{40}, c_{42}, and c_{44} are the components of a fourth-rank irreducible tensor. Thus we can break up Eq. 1 as $U(\beta,\gamma) = U^{(2)}(\beta,\gamma) + U^{(4)}(\beta,\gamma)$, where $U^{(2)}$ contains terms involving the $c_{2,\bar{K}}$ and $U^{(4)}$ contains terms involving the $c_{4,\bar{K}}$. It then follows that

$$-U^{(2)}_{zz} \equiv -U^{(2)}(0, 0) = c_{20}$$

$$-U^{(2)}_{xx} \equiv -U^{(2)}(\pi/2, 0) = -c_{20}/2 + (3/2)^{1/2} c_{22}$$

$$-U^{(2)}_{yy} \equiv -U^{(2)}(\pi/2, \pi/2) = -c_{20}/2 - (3/2)^{1/2} c_{22}$$

Alternatively, $c_{20} = -U^{(2)}_{zz}$ and $c_{22} = (U^{(2)}_{yy} - U^{(2)}_{xx})/6^{1/2}$. If we now permute axes as follows: $y \rightarrow \hat{z}$, $z \rightarrow \hat{x}$, and $x \rightarrow \hat{y}$, then $U_{yy} \rightarrow U_{\hat{z}\hat{z}}$, etc. In the new axis system represented by the carets, we then find from the above that

$$\hat{c}_{20} = -c_{20}/2 - (3/2)^{1/2} c_{22}$$

$$\hat{c}_{22} = ((3/2)^{1/2} c_{20} - c_{22})/2$$

In a similar manner, we obtain from $U^{(4)}$

$$-U^{(4)}_{zz} = c_{40}$$

$$-U^{(4)}_{xx} = (3/8)c_{40} - (5/8)^{1/2} c_{42} + (35/32)^{1/2} c_{44}$$

$$-U^{(4)}_{yy} = (3/8)c_{40} + (5/8)^{1/2} c_{42} + (35/32)^{1/2} c_{44}$$

and thus $c_{40} = -U^{(4)}_{zz}$, $c_{42} = (2/5)^{1/2}(U^{(4)}_{xx} - U^{(4)}_{yy})$, and $c_{44} = (8/35)^{1/2}(-U^{(4)}_{xx} - U^{(4)}_{yy} + (3/4)U^{(4)}_{zz})$. When the axes are permuted as above, we obtain

$$\hat{c}_{40} = (3/8)c_{40} + (5/8)^{1/2} c_{42} + (35/32)^{1/2} c_{44}$$

$$\hat{c}_{42} = -(5/32)^{1/2} c_{40} - (1/2)c_{42} + (7/16)^{1/2} c_{44}$$

$$\hat{c}_{44} = c_{44}$$

Note that if $c_{44} = 0$, then $\hat{c}_{44} = 0$, which is the case in our analysis.

Note also that, for the orientations described in Fig. 6, $U(\textit{upright}) = U_{yy} \equiv U^{(2)}_{yy} + U^{(4)}_{yy}$, $U(\textit{sideways}) = U_{zz}$, $U(\textit{facedown}) = U_{xx}$, and $U(\textit{barrier}) = U(\beta = \pi/4, \gamma = \pi/2)$.

We acknowledge helpful discussions with Dr. Mingtao Ge, Dr. Keith Earle, and David Schneider.

This work was supported by National Institutes of Health grants GM25862 and RR07216 and National Science Foundation grant CHE9615910. JPB was partially supported by a National Research Service Award (GM17174). The computations were performed at the Cornell Theory Center.

REFERENCES

Abragam, A. 1961. Principles of Nuclear Magnetism. Oxford University Press, New York. 442–451.

Adam, G., and M. Delbrück. 1968. Reduction of dimensionality in biological diffusion processes. *In* Structural Chemistry and Molecular Biology. A. Rich and N. Davidson, editors. W. H. Freeman and Co., San Francisco. 198–215.

Asher, S. A., and P. S. Pershan. 1979. Alignment and defect structures in oriented phosphatidylcholine multilayers. *Biophys. J.* 27:393–421.

Balvers, W. G., M. G. Boersma, J. Vervoort, A. Ouwehand, and I. Rietjens. 1993. A specific interaction between NADPH-cytochrome reductase and phosphatidylserine and phosphatidylinositol. *Eur. J. Biochem.* 218: 1021–1029.

Barnes, J. P., and J. H. Freed. 1997. An aqueous sample holder for high frequency electron spin resonance. *Rev. Sci. Instrum.* 68:2838–2846.

Barnes, J. P., and J. H. Freed. 1998. A "shunt" Fabry-Perot resonator for high frequency electron spin resonance utilizing a variable coupling scheme. *Rev. Sci. Instrum.* 69:3022–3027.

Berggren, E., and C. Zannoni. 1995. Rotational diffusion of biaxial probes in biaxial liquid crystal phases. *Mol. Phys.* 85:299–333.

Boggs, J. 1987. Lipid intermolecular hydrogen bonding: influence on structural organization and membrane function. *Biochim. Biophys. Acta.* 906:353–404.

Bordeaux, P. D., and J. Lajzérowicz-Bonneteau. 1974. Structure cristalline du spiro[cyclohexane-1,2′-(diméthyl-4′,4′-oxazolidine)]. *Acta Crystallogr. B.* 30:2130–2132.

Brasaemle, D. L., A. D. Robertson, and A. D. Attie. 1988. Transbilayer movement of cholesterol in the human erythrocyte membrane. *J. Lipid Res.* 29:481–489.

Brumm, T., A. Möps, C. Dolainsky, S. Brückner, and T. Bayerl. 1992. Macroscopic orientation effects in broadline NMR spectra of model membranes at high magnetic field strength. *Biophys. J.* 61:1018–1024.

Budil, D. E., K. A. Earle, W. B. Lynch, and J. H. Freed. 1989. Electron paramagnetic resonance at 1 millimeter wavelengths. *In* Advanced EPR: Applications in Biology and Biochemistry. A. J. Hoff, editor. Elsevier, Amsterdam. 307–340.

Budil, D. E., S. Lee, S. Saxena, and J. H. Freed. 1996. Nonlinear-least-squares analysis of slow-motional EPR spectra in one and two dimensions using a modified Levenberg-Marquardt algorithm. *J. Magn. Reson. A.* 120:155–189.

Campbell, R. F., E. Meirovitch, and J. H. Freed. 1979. Slow motional NMR line shapes for very anisotropic rotational diffusion. Phosphorus-31 NMR of phospholipids. *J. Phys. Chem.* 83:525–533.

Cascales, L. J. J., and J. García de la Torre. 1997. Effect of lithium and sodium ions on a charged membrane of dipalmitoylphosphatidylserine: a study by molecular dynamics simulation. *Biochim. Biophys. Acta.* 1330:145–156.

Clark, N. A., K. J. Rothschild, D. A. Luippold, and B. A. Simon. 1980. Surface-induced lamellar orientation of multilayer membrane arrays. *Biophys. J.* 31:65–96.

Dreger, M., M. Krauss, A. Herrmann, and F. Hucho. 1997. Interactions of the nicotinic acetylcholine receptor transmembrane segments with the lipid bilayer in native receptor-rich membranes. *Biochemistry.* 36: 839–847.

Earle, K. A., D. E. Budil, and J. H. Freed. 1993. 250 GHz EPR of nitroxides in the slow motional regime: models of rotational diffusion. *J. Phys. Chem.* 97:13289–13297.

Earle, K. A., D. E. Budil, and J. H. Freed. 1996. Millimeter wave electron spin resonance using quasioptical techniques. *In* Advances in Magnetic and Optical Resonance. W. S. Warren, editor. Academic Press, San Diego. 253–321.

Earle, K. A., J. K. Moscicki, M. Ge, D. E. Budil, and J. H. Freed. 1994. 250 GHz electron spin resonance studies of polarity gradients along the aliphatic chains in phospholipid membranes. *Biophys. J.* 66:1213–1221.

Earle, K. A., J. K. Moscicki, A. Polimeno, and J. H. Freed. 1997. A 250 GHz ESR study of *o*-terphenyl: dynamic cage effects above T_c. *J. Chem. Phys.* 106:9996–10015.

Feigenson, G. W. 1989. Calcium ion binding between lipid bilayers: the four-component system of phosphatidylserine, phosphatidylcholine, calcium chloride, and water. *Biochemistry.* 28:1270–1278.

Freed, J. H., A. Nayeem, and S. B. Rananavare. 1994. ESR and liquid crystals: statistical mechanics and generalised Smoluchowski equations. *In* The Molecular Dynamics of Liquid Crystals. G. R. Luckhurst and C. A. Veracini, editors. Kluwer Academic Publishers, Dordrecht, the Netherlands. 71–84.

Ge, M., D. B. Budil, and J. H. Freed. 1994a. ESR studies of spin-labeled membranes aligned by isopotential spin-dry ultracentrifugation: lipid-protein interactions. *Biophys. J.* 67:2326–2344.

Ge, M., D. Budil, and J. H. Freed. 1994b. An electron spin resonance study of interactions between phosphatidylcholine and phosphatidylserine in oriented membranes. *Biophys. J.* 66:1515–1521.

Ge, M., and J. H. Freed. 1998. Polarity profiles in oriented and dispersed phosphatidylcholine bilayers are different: an electron spin resonance study. *Biophys. J.* 74:910–917.

Hauser, H. 1984. Some aspects of the phase behavior of charged lipids. *Biochim. Biophys. Acta.* 772:37–50.

Hauser, H., and G. G. Shipley. 1983. Interactions of monovalent cations with phosphatidylserine bilayer membranes. *Biochemistry.* 22: 2171–2178.

Heimburg, T., and D. Marsh. 1995. Protein surface-distribution and protein-protein interactions in the binding of peripheral proteins to charged lipid membranes. *Biophys. J.* 68:536–546.

Hinderliter, A. K., J. Huang, G. Feigenson. 1994. Detection of phase separation in fluid phosphatidylserine/phosphatidylcholine mixtures. *Biophys. J.* 67:1906–1911.

Ipsen, J. H., G. Karlström, O. G. Mouritsen, H. Wennerström, and M. J. Zuckermann. 1987. Phase equilibria in the phosphatidylcholine-cholesterol system. *Biochim. Biophys. Acta.* 905:162–172.

Ishida, T., M. Inoue, S. Harusawa, Y. Hamada, and T. Shioiri. 1981. New methods in reagents in organic synthesis. XIII. Structure of 3β-(1-pyrrolidinyl)-5α-cholestane-3α-carbonitrile. *Acta Crystallogr. B.* 37: 1881–1884.

Kar, L., E. Ney-Igner, and J. H. Freed. 1985. Electron spin resonance and electron spin echo study of oriented multilayers of L_α dipalmitoylphosphatidylcholine water systems. *Biophys. J.* 48:569–595.

Kittel, C. 1976. Introduction to Solid State Physics, 5th Ed. John Wiley and Sons, New York. 424.

Kleinschmidt, J. H., and D. Marsh. 1997. Spin-label electron spin resonance studies on the interactions of lysine peptides with phospholipid membranes. *Biophys. J.* 73:2546–2556.

Kohler, S. J., and M. P. Klein. 1977. Orientation and dynamics of phospholipid head groups in bilayers and membranes determined from ^{31}P nuclear magnetic resonance chemical shielding tensors. *Biochemistry.* 16:519–526.

Marriott, T. B., G. B. Birrell, and O. H. Griffith. 1975. Assignment of the configuration of the steroid spin label, 3-doxyl- 5α-cholestane. *J. Am. Chem. Soc.* 97:627–630.

Marsh, D. 1988. The CRC Handbook of Lipid Bilayers. Chapter 2. CRC Press, Boca Raton, FL.

McLaughlin, S., and A. Aderem. 1995. The myristoyl-electrostatic switch: a modulator of reversible protein-membrane interactions. *Trends Biol. Sci.* 20:272–276.

McMullen, T. P. W., and R. N. McElhaney. 1997. Differential scanning calorimetric studies of the interaction of cholesterol with distearoyl and dielaidoyl molecular species of phosphatidylcholine, phosphatidylethanolamine, and phosphatidylserine. *Biochemistry.* 36:4979–4986.

Meirovitch, E., and J. H. Freed. 1980. ESR studies of low water content 1,2-dipalmitoyl-*sn*-glycero-3-phosphocholine in oriented multilayers. 2. Evidence for magnetic field induced reorientation of the polar headgroups. *J. Phys. Chem.* 84:3295–3303.

Meirovitch, E., D. Igner, E. Igner, G. Moro, and J. H. Freed. 1982. Electron-spin relaxation and ordering in smectic and supercooled nematic liquid crystals. *J. Chem. Phys.* 77:3915–3938.

Meirovitch, E. 1983. Electron spin resonance observations on the annealing process of low-water-content dipalmitoylphosphatidylcholine bilayers. *J. Phys. Chem.* 87:845–850.

Mitchell, D., and B. Litman. 1998. Molecular order and dynamics in bilayers consisting of highly polyunsaturated phospholipids. *Biophys. J.* 74:879–891.

Mou, J., D. M. Czajkowsky, and Z. Shao. 1996. Gramicidin A aggregation in supported gel state phosphatidylcholine bilayers. *Biochemistry.* 35: 3222–3226.

Patyal, B. R., R. H. Crepeau, and J. H. Freed. 1997. Lipid-gramicidin interactions using two-dimensional Fourier-transform electron spin resonance. *Biophys. J.* 73:2201–2220.

Powers, L., and N. A. Clark. 1975. Preparation of large monodomain phospholipid bilayer smectic liquid crystals. *Proc. Nat. Acad. Sci. USA.* 72:840–843.

Recktenwald, D. J., and H. M. McConnell. 1981. Phase equilibria in binary mixtures of phosphatidylcholine and cholesterol. *Biochemistry.* 20: 4505–4510.

Roux, M., and M. Bloom. 1990. Ca^{2+}, Mg^{2+}, Li^+, Na^+, and K^+ distributions in the headgroup region of binary membranes of phosphatidylcholine and phosphatidylserine as seen by deuterium NMR. *Biochemistry.* 29:7077–7089.

Roux, M., J.-M. Neumann, R. S. Hodges, P. F. Devaux, and M. Bloom. 1989. Conformational changes of phospholipid headgroups induced by a cationic integral membrane peptide as seen by deuterium magnetic resonance. *Biochemistry.* 28:2313–2321.

Sanson, A., M. A. Monck, and J.-M. Neumann. 1995. 2D ^{1}H-NMR conformational study of phosphatidylserine diluted in perdeuterated dodecylphosphocholine micelles. Evidence for a pH-induced conformational transition. *Biochemistry.* 34:5938–5944.

Schneider, D. J., and J. H. Freed. 1989. Calculating slow motional magnetic resonance spectra: a user's guide. *In* Biological Magnetic Resonance, Vol. 8, Spin Labeling, Theory and Application. L. J. Berliner and J. Reuben, editors. Plenum Press, New York. 1–76.

Schneider, K.-P., and J. Keller. 1997. Computer simulation of the orientation of lipid headgroups. *Chem. Phys. Lett.* 275:63–69.

Shieh, H.-S., L. Hoard, and C. Nordman. 1981. The structure of cholesterol. *Acta. Crystallogr. B.* 37:1538–1543.

Shin, Y.-K., D. Budil, and J. H. Freed. 1993. Thermodynamics and dynamics of phosphatidylcholine-cholesterol mixed model membranes in the liquid crystalline state: effects of water. *Biophys. J.* 65:1283–1294.

Shin, Y.-K., and J. H. Freed. 1989. Thermodynamics of phosphatidylcholine-cholesterol mixed model membranes in the liquid crystalline state studied by the orientational order parameter. *Biophys. J.* 56:1093–1100.

Silvius, J. R. 1992. Cholesterol modulation of lipid intermixing in phospholipid and glycosphingolipid mixtures. Evaluation using fluorescent lipid probes and brominated lipid quenchers. *Biochemistry.* 31:3398–3408.

Simons, K., and E. Ikonen. 1997. Functional rafts in cell membranes. *Nature.* 387:569–572.

Sintes, T., and A. Baumgärtner. 1997. Protein attraction in membranes induced by lipid fluctuations. *Biophys. J.* 73:2251–2259.

Speyer, J. B., P. K. Sripada, S. K. Das Gupta, and G. G. Shipley. 1987. Magnetic orientation of sphingomyelin-lecithin bilayers. *Biophys. J.* 51:687–691.

Sun, W.-J., R. M. Suter, M. A. Knewtson, C. R. Worthington, S. Tristram-Nagle, R. Zhang, and J. F. Nagle. 1994. Order and disorder in fully hydrated unoriented bilayers of gel phase dipalmitoylphosphatidylcholine. *Phys. Rev. E.* 49:4665–4676.

Takahashi, H., H. Ohmae, and I. Hatta. 1997. Trehalose-induced destabilization of interdigitated gel phase in dihexadecylphosphatidylcholine. *Biophys. J.* 73:3030–3038.

Tanford, C. 1980. The Hydrophobic Effect: Formation of Micelles and Biological Membranes, 2nd Ed. John Wiley, New York.

Tokutomi, S., K. Ohki, and S. Ohnishi. 1980. Proton-induced phase separation of phosphatidylserine phosphatidylcholine membranes. *Biochim. Biophys. Acta.* 596:192–200.

Vergères, G., S. Manenti, T. Weber, and C. Stürzinger. 1995. The myristoyl moiety of myristoylated alanine-rich C Kinase substrate (MARCKS) and MARCKS-related protein is embedded in the membrane. *J. Biol. Chem.* 270:19879–19887.

Wachtel, E. J., N. Borochov, and D. Bach. 1991. The effect of protons or calcium ions on the phase behavior of phosphatidylserine-cholesterol mixtures. *Biochim. Biophys. Acta.* 1066:63–69.

Yang, L., and M. Glaser. 1995. Membrane domains containing phosphatidylserine and substrate can be important for the activation of protein kinase C. *Biochemistry.* 34:1500–1506.

Yeagle, P. L. 1991. The dynamics of membrane lipids. *In* The Structure of Biological Membranes. P. Yeagle, editor. CRC Press, Boca Raton, FL. 157–174.

Yeagle, P., A. Albert, K. Boesze-Battaglia, J. Young, and J. Frye. 1990. Cholesterol dynamics in membranes. *Biophys. J.* 57:413–424.

Zachowski, A. 1993. Phospholipids in animal eukaryotic membranes: transverse asymmetry and movement. *Biochem. J.* 294:1–14.